Photovoltaics

DOI: 10.1002/ange.201301776

Photovoltaic Wire Derived from a Graphene Composite Fiber Achieving an 8.45% Energy Conversion Efficiency**

*Zhibin Yang, Hao Sun, Tao Chen, Longbin Qiu, Yongfeng Luo, and Huisheng Peng**

Photovoltaic devices are typically made of rigid plates that are unfavorable for applications that require flexibility, for example, portable and highly integrated devices. Therefore, the development of flexible organic photovoltaics has recently become the subject of research as a possible solution for these applications.[1,2] However, the flexible films described do not meet many of the requirements, for example, they are not weaveable and cannot be used for electronic textiles, which represent a mainstream future development. As a result, flexible wire devices have begun to attract attention, and some attempts to make wire-shaped photovoltaics have been discussed in the recent years.[3–10] However, photovoltaic wires suffer from poor performance and generally exhibit much lower energy-conversion efficiency than conventional planar photovoltaics; the metal wire, carbon fiber, or modified polymer fiber commonly used as electrodes are generally unable to fully meet the much stricter requirements of wire-based cells, including a complex interface, high flexibility, and high conductivity.[3,5,11]

Graphene, a single atomic layer of graphite, has attracted increasing interest owing to its remarkable properties.[12–25] However, it is rare to prepare graphene materials in the form of a one-dimensional fiber,[26–28] although a continuous fiber would be very useful in both traditional and modern industries as well as for the development of nanomaterials.[29–33]

In the present study, we spun graphene into flexible fibers using a low-cost and effective solution process. The fiber exhibited a density of 0.61 $g\,cm^{-3}$, a strength of 10^2–10^3 MPa, and an electrical conductivity of 10^2–10^3 $S\,cm^{-1}$. The graphene fiber could be electrodeposited with platinum nanoparticles to serve as a counter electrode, and a titanium wire impregnated with perpendicularly aligned titania nanotubes functioned as the working electrode. The two electrodes were twisted together to produce dye-sensitized photovoltaic wires that could effectively capture incident light coming from any direction. The high flexibility, mechanical strength, and electrical conductivity of graphene composite fibers resulted in a certified maximum energy conversion efficiency of 8.45%, which is the recorded efficiency for the wire-shaped photovoltaic devices.

To synthesize the graphene fibers, aqueous dispersions of graphene oxide (GO) were first synthesized using a modified Hummer's method. Figure S1a and S1b in the Supporting Information show typical transmission electron microscopy (TEM) images of GO sheets. The GO sheets have widths of less than 2 μm and an average thickness of approximately 1.1 nm (Figure S1c and S1d). The GO fibers were then prepared using a wet spinning method (Figures S2 and S3). The diameter of the fiber could be tuned by varying the inner diameter of the nozzle and the drawing speed. With this approach, an inner diameter of 300 mm produced GO fibers with a diameter of 40 mm after drying. The density of GO fibers was calculated to be 1.15 $g\,cm^{-3}$. Graphene fibers were finally obtained by a chemical reduction of GO fibers using hydroiodic acid (40%). The fibers shrank to 31 mm in diameter with a concomitant reduction in density of 0.61 $g\,cm^{-3}$. The reduction of GO was confirmed by Raman spectroscopy (Figure S4). The intensity ratio of D to G bands increased from 0.85 to 1.21, and the 2D band appeared following the reduction, which may be attributed to more disordered graphene edges owing to the elimination of pendant functional groups in the GO sheets.

Figure 1a and b show typical scanning electron microscopy (SEM) images of a continuous and uniform graphene fiber at different magnification levels. Figure S5 further reveals that the graphene fibers could be made into a tight knot, which indicates their good flexibility and high mechanical strength. The mechanical properties of GO and graphene fibers are further shown in Figure S6. The tensile strength of the graphene fiber was approximately 330 MPa, much higher than around 100 MPa observed for the GO fiber. This greatly enhanced mechanical strength can be explained by the fact that the graphene sheets are more closely stacked, for example, the fibers shrank after the reduction. The cross section of a broken graphene fiber under tensile forces further confirmed its highly stacked structure (Figure 1c). The electrical properties of GO and graphene fibers were also compared. The GO fibers were almost insulating, whereas the graphene fiber showed a high conductivity of around 200 $S\,cm^{-1}$ at room temperature. Figure S7 further shows that the conductivity increases with the increasing temperature from 10 to 373 K, which is indicative of semiconductor behavior.[34]

The combined remarkable mechanical and electrical properties confirm that the graphene fibers are a new family of electrode materials. Next, their use as counter-

[*] Z. Yang, H. Sun, Dr. T. Chen, L. Qiu, Dr. Y. Luo, Prof. H. Peng
State Key Laboratory of Molecular Engineering of Polymers, Department of Macromolecular Science, and Laboratory of Advanced Materials, Fudan University
Shanghai 200438 (China)
E-mail: penghs@fudan.edu.cn

[**] This work was supported by NSFC (91027025, 21225417), MOST (2011CB932503, 2011DFA51330), STCSM (11520701400, 12nm0503200), Fok Ying Tong Education Foundation and The Program for Prof. of Special Appointment at Shanghai Institutions of Higher Learning.

Supporting information for this article is available on the WWW under http://dx.doi.org/10.1002/anie.201301776.

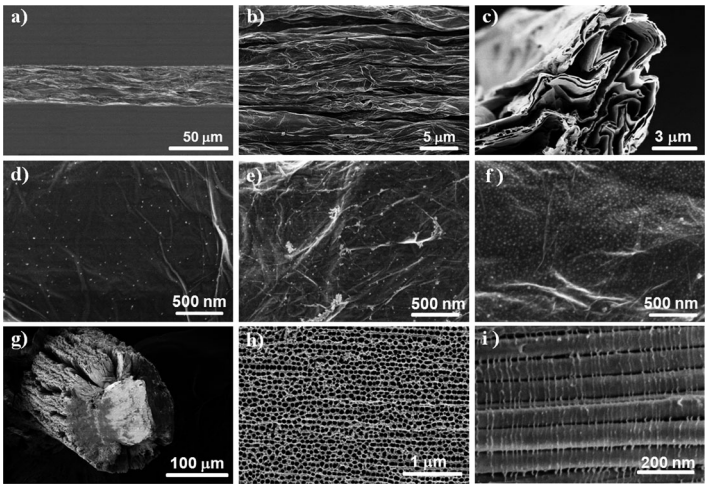

Figure 1. Scanning electron microscopy (SEM) images of bare graphene fibers, graphene/Pt composite fibers, and TiO_2 nanotube-modified Ti wires. a) and b) A graphene fiber at different magnifications. c) Cross-sectional view of a graphene fiber after failure during the mechanical test. d)–f) Side views of graphene/Pt composite fibers with increasing Pt contents of 4.6%, 7.1% and 22.9%, respectively. g) Cross-sectional view of a Ti wire grown with TiO_2 nanotube arrays on the surface. h) and i) Top and side views of aligned TiO_2 nanotubes.

electrode materials in dye-sensitized solar cells was investigated. To this end, the graphene fibers were modified with platinum (Pt) nanoparticles to further increase the catalytic activity. Owing to their high conductivity, graphene fibers can be easily electrodeposited with uniform Pt nanoparticles on the surface using a double potential step electrochemical method, and the weight percentage of Pt can be controlled by varying the deposition time.[35] For instance, the weight percentage of Pt increased from 2.6 to 22.9% by increasing the electrodepositing time from 10 to 500 s (Figure S8). The Pt nanoparticles were nearly the same in diameter (ca. 12 nm). Figure 1d–f show the surface morphologies of graphene/Pt composite fibers prepared using an increasing Pt content of 4.6, 7.1, and 22.9%, respectively. Accordingly, the conductivity also increased (Figure S9) to 1024 $S\,cm^{-1}$ for 22.9% Pt. The mechanical properties, including the tensile strengths of the composite fibers, remained nearly unchanged.

For the fabrication of dye-sensitized photovoltaic wires, titanium wires were grown with a layer of perpendicularly aligned titania nanotubes on the surface. The anodizing method was used to produce the working electrode (Figure 1g).[4,36] Figure 1h and i show the structure of TiO_2 nanotubes from top and side views. The diameters of TiO_2 nanotubes ranged from 70 to 100 nm, and the lengths of the TiO_2 nanotubes were varied by changing the anodizing time. After the adsorption of N719 (Figure S10), the working electrode was twined with the graphene/Pt composite fiber, then the electrolytes were introduced (see the Supporting information for the detailed fabrication procedure).

The catalytic activity of graphene fiber, graphene/Pt composite fibers, and Pt wire was compared by cyclic voltammetry. Figure 2a shows typical cyclic voltammograms for the fibers prepared using different Pt concentrations. Two pairs of oxidation/reduction peaks can be observed in each curve, with the left pair corresponding to the redox reaction of I_3^-/I^- (see Supporting Information for experimental details). Generally, higher peak current densities and lower peak-to-peak voltage separations (V_{PP}) indicate improved catalytic activities for counter electrodes.[37] As graphene/Pt composite fibers with high surface areas produced high current densities, the catalytic activity had been determined by comparing the V_{PP} values between the two peaks. As shown in Figure 2a, the V_{PP} decreased from 0.75 to 0.3 V as the Pt content increased from 0 to 7.1% and became stable at 0.3 V with further increase in Pt content (Figure 2a). In comparison, the Pt wire exhibited a V_{pp} of 0.42 V. A lower V_{PP} value indicates that the composite fiber has a higher capability for the reduction of I_3^-.

Figure 3a schematically shows the structure of a typical dye-sensitized photovoltaic wire, and photographs of two real cells are provided in Figure 3b–d. Figure 2b shows the *J*–*V* characteristics measured under AM 1.5 illumination for the wires prepared using graphene/Pt composite fibers with different Pt content as the counter electrodes and a Ti wire with TiO_2 nanotubes of 30 μm in length as the working electrode. The photovoltaic parameters are given in Table S1. The open-circuit voltage (V_{OC}) remained nearly the same at 0.73 V, whereas the short-circuit current density (J_{SC}) and the fill factor (FF) increased from 12.67 to 17.11 $mA\,cm^{-2}$ and 0.42 to 0.67 when the Pt content increased from 0 to 7.1%, respectively. All three parameters remained unchanged with a further increase in the concentration of Pt. In other words, the energy conversion efficiency (h) achieved a maximum at a Pt loading of 7.1%. The efficiency achieved a stable value of 8.41%. In comparison, a photovoltaic prepared with a Pt wire as the counter electrode exhibited a maximum efficiency of 7.22%. To summarize, the photovoltaic wire based on graphene/Pt composite fibers exhibited efficiencies in the range of 8.20–8.61%, whereas those of Pt wires achieved efficiencies of 7.06–7.31%. To elucidate the obtained J_{sc} values in the wire cell, the incident photon-to-electron conversion efficiency was measured as a function of wavelength (Figure S11). A maximum of 85% was obtained at a wavelength of 530 nm. The energy conversion efficiency was certified with a value of 8.45% (Figure S12).

To further understand the high performance of the graphene/Pt composite fibers as counter electrodes, electrochemical impedance spectroscopy (EIS) was performed (see Figure S13 for the equivalent circuit). As shown in Figure 2c, two semicircles were typically observed in the Nyquist plot. The first semicircle represents the electrochemical reaction at the counter electrode in the high-frequency region (i.e., R_{CT1}) and the Nernst diffusion impedance in the pore of the graphene/Pt composite fiber (i.e., $Z_{W,pore}$), whereas the second semicircle reflects the charge transfer (CT) at the TiO_2/dye/electrode interfaces in the middle-frequency region (i.e., R_{CT2}) and the Warburg diffusion process of I^- and I_3^- ions in the electrolyte in the low-frequency region (i.e., R_{diff}).[12,14,38,39] The measurement was performed after the electrolyte had been infiltrated into the composite fiber, and the $Z_{W,pore}$ part could be neglected. The first semicircle mainly corresponded

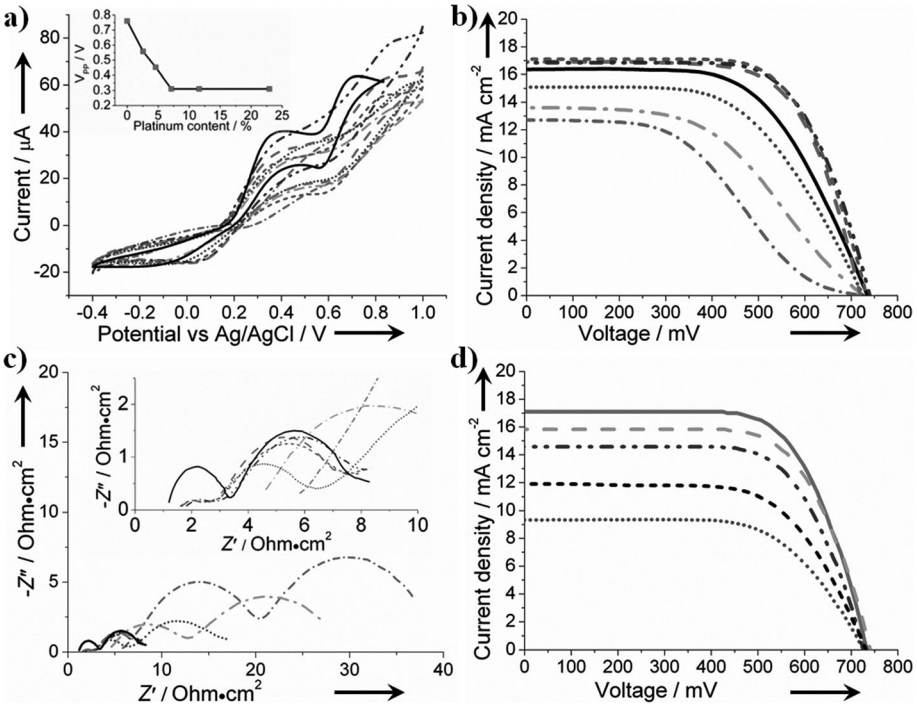

Figure 2. a) Electrocatalytic characterization of graphene/Pt composite fibers with increasing Pt content. 22.9% (–––); 11.6% (-----); 7.1% (–··–); 4.6% (••••); 2.5% (–•–•); 0% (–·–·–); Pt (——). The insert shows the peak-to-peak voltage separation (V_{PP}) in the graphene/Pt composite fibers as a function of Pt electrodepositing time. b) *J*–*V* characteristics of the wire cell prepared using graphene/Pt composite fiber counter electrodes with the increasing Pt content and modified Ti wire (TiO_2 nanotubes with a length of 30 μm) working electrodes measured under AM 1.5 illumination. (22.9% (–––); 11.6% (-----); 7.1% (–··–); 4.6% (••••); 2.5% (–•–•); 0% (–·–·–); Pt (——). c) Nyquist plots of the wire cells in (a). The inserted image shows a magnified section, and the frequencies range from 0.1 to 100 kHz with an applied voltage of −0.8 V. (22.9% (–––); 11.6% (-----); 7.1% (–··–); 4.6% (••••); 2.5% (–•–•); 0% (–·–·–); Pt (——). d) *J*–*V* characteristics of the wire cells with increasing lengths of TiO_2 nanotubes in working electrodes and graphene/Pt composite fibers (Pt content of 7.1%) as counter electrodes measured under AM 1.5 illumination. Approximate length: 10 μm (••••); 15 μm (-----); 23 μm (–··–); 30 μm (——); 40 μm (–––).

to the R_{CT1} which reflected the catalytic activity of the counter electrode. In Figure 2c, the R_{CT1} generally decreased as the Pt content increased from 0 to 22.9% and confirmed a value of 0.3 Ω cm^2 at 7.1–22.9%, which is much lower than the 1.1 Ω cm^2 observed for the Pt wire. At the same time, both R_{CT2} and R_{diff} also decreased to produce lower total resistances and higher energy conversion efficiencies.

To optimize the wire, the dependence of the photovoltaic parameter on the length of the titania nanotubes was investigated (Figure 2d). Both V_{OC} and the FF were maintained at appropriately 0.73 V and 0.67 as the length of the titania nanotubes increased from 10 to 40 μm, respectively. In contrast, J_{SC} first increased from 9.34 to 17.11 mA cm^{-2} with the increasing nanotube length from 10 to 30 μm and then decreased to 15.84 mA cm^{-2} with the further increase to 40 μm. The first increase in the J_{SC} is mainly due to the fact that longer titania nanotubes absorb more N719 dyes, which generates more photoelectrons. However, when the titania nanotubes exceeded the photon penetration and the electron diffusion lengths, the charge recombination increased, whereas the electron collection efficiency decreased, resulting in lower J_{SC} values. The detailed parameters are summarized in Table S2, and an optimal length of 30 μm was observed. In addition, the efficiency was maintained by increasing the cell length, which is important for practical applications (Figure S14).

These wires exhibit several unique advantages. For instance, the energy conversion efficiency is independent of the incident light angle (Figure S15), which enables these wires to more effectively take advantage of the solar energy. owing to their high flexibility and stability, these wires could be easily woven with one another to produce electronic textiles or could be integrated into textiles made of various synthetic fibers.

In summary, we have developed novel wire-shaped photovoltaic devices based on graphene/Pt composite fibers. The high flexibility, mechanical strength and electrical conductivity of graphene fibers resulted in a certified maximum energy conversion efficiency of 8.45%, which is much higher than that of other wire-shaped photovoltaic devices (Figure S16). These photovoltaic wires have the potential to be easily woven into clothes, packages, and other portable devices to serve as self-powered electric

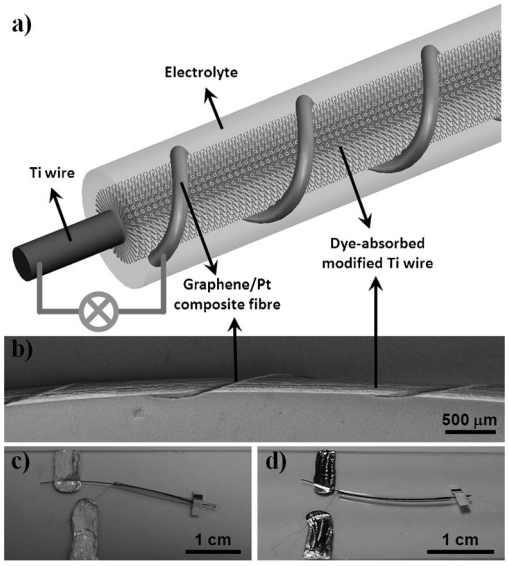

Figure 3. Dye-sensitized photovoltaic wire prepared by using a graphene/Pt composite fiber as the counter electrode and a Ti wire impregnated with TiO_2 nanotubes as the working electrode. a) Schematic illustration. b) SEM image. c) and d) Photographs of photovoltaic wires sealed in a capillary glass tube and flexible fluorinated ethylene propylene tube, respectively.

generators, by the conventional textile technology. This work also provides a new fabrication approach in the development of new photovoltaic materials and devices.

Received: March 1, 2013
Revised: March 31, 2013
Published online: May 28, 2013

Keywords: graphene fiber · photovoltaic wire · platinum

[1] S. I. Na, S. S. Kim, J. Jo, D. Y. Kim, *Adv. Mater.* **2008**, *20*, 4061 – 4067.
[2] H. Lindström, A. Holmberg, E. Magnusson, S. E. Lindquist, L. Malmqvist, A. Hagfeldt, *Nano Lett.* **2001**, *1*, 97 – 100.
[3] B. Weintraub, Y. Wei, Z. L. Wang, *Angew. Chem.* **2009**, *121*, 9143 – 9147; *Angew. Chem. Int. Ed.* **2009**, *48*, 8981 – 8985.
[4] T. Chen, L. Qiu, H. G. Kia, Z. Yang, H. Peng, *Adv. Mater.* **2012**, *24*, 4623 – 4628.
[5] M. R. Lee, R. D. Eckert, K. Forberich, G. Dennler, C. J. Brabec, R. A. Gaudiana, *Science* **2009**, *324*, 232 – 235.
[6] T. Chen, L. Qiu, Z. Cai, F. Gong, Z. Yang, Z. Wang, H. Peng, *Nano Lett.* **2012**, *12*, 2568 – 2572.
[7] Y. Fu, Z. Lv, S. Hou, H. Wu, D. Wang, C. Zhang, Z. Chu, X. Cai, X. Fan, Z. L. Wang, *Energy Environ. Sci.* **2011**, *4*, 3379 – 3383.
[8] T. Chen, L. Qiu, Z. Yang, H. Peng, *Chem. Soc. Rev.* **2013**, DOI: 10.1039/C3CS35465B.
[9] T. Chen, L. Qiu, Z. Yang, Z. Cai, J. Ren, H. Li, H. Lin, X. Sun, H. Peng, *Angew. Chem.* **2012**, *124*, 12143 – 12146; *Angew. Chem. Int. Ed.* **2012**, *51*, 11977 – 11980.
[10] T. Chen, L. Qiu, H. Li, H. Peng, *J. Mater. Chem.* **2012**, *22*, 23655 – 23658.
[11] S. Hou, X. Cai, Y. Fu, Z. Lv, D. Wang, H. Wu, C. Zhang, Z. Chu, D. Zou, *J. Mater. Chem.* **2011**, *21*, 13776 – 13779.
[12] J. D. Roy-Mayhew, D. J. Bozym, C. Punckt, I. A. Aksay, *ACS Nano* **2010**, *4*, 6203.
[13] A. A. Balandin, S. Ghosh, W. Bao, I. Calizo, D. Teweldebrhan, F. Miao, C. N. Lau, *Nano Lett.* **2008**, *8*, 902 – 907.
[14] L. Kavan, J.-H. Yum, M. Grätzel, *Nano Lett.* **2011**, *11*, 5501 – 5506.
[15] L. Kavan, J.-H. Yum, M. Graetzel, *ACS Appl. Mater. Interfaces* **2012**, *4*, 6999 – 7006.
[16] K. Novoselov, A. Geim, S. Morozov, D. Jiang, M. I. K. I. V. Grigorieva, S. Dubonos, A. Firsov, *Nature* **2005**, *438*, 197 – 200.
[17] Y. Zhang, Y. W. Tan, H. L. Stormer, P. Kim, *Nature* **2005**, *438*, 201 – 204.
[18] C. Lee, X. Wei, J. W. Kysar, J. Hone, *Science* **2008**, *321*, 385 – 388.
[19] K. Novoselov, A. Geim, S. Morozov, D. Jiang, Y. Zhang, S. Dubonos, I. Grigorieva, A. Firsov, *Science* **2004**, *306*, 666 – 669.
[20] N. Yang, J. Zhai, D. Wang, Y. Chen, L. Jiang, *ACS Nano* **2010**, *4*, 887 – 894.
[21] V. Gupta, N. Chaudhary, R. Srivastava, G. D. Sharma, R. Bhardwaj, S. Chand, *J. Am. Chem. Soc.* **2011**, *133*, 9960 – 9963.
[22] X. Wang, L. Zhi, K. Müllen, *Nano Lett.* **2008**, *8*, 323 – 327.
[23] X. Yan, X. Cui, B. Li, L. Li, *Nano Lett.* **2010**, *10*, 1869 – 1873.
[24] F. Schedin, A. Geim, S. Morozov, E. Hill, P. Blake, M. Katsnelson, K. Novoselov, *Nat. Mater.* **2007**, *6*, 652 – 655.
[25] I. Meric, M. Y. Han, A. F. Young, B. Ozyilmaz, P. Kim, K. L. Shepard, *Nat. Nanotechnol.* **2008**, *3*, 654 – 659.
[26] Z. Dong, C. Jiang, H. Cheng, Y. Zhao, G. Shi, L. Jiang, L. Qu, *Adv. Mater.* **2012**, *24*, 1856 – 1861.
[27] Z. Xu, C. Gao, *Nat. Commun.* **2011**, *2*, 571.
[28] X. Li, P. Sun, L. Fan, M. Zhu, K. Wang, M. Zhong, J. Wei, D. Wu, Y. Cheng, H. Zhu, *Sci. Rep.* **2012**, *2*, 395.
[29] L. M. Ericson, H. Fan, H. Peng, V. A. Davis, W. Zhou, J. Sulpizio, Y. Wang, R. Booker, J. Vavro, C. Guthy, *Science* **2004**, *305*, 1447 – 1450.
[30] M. Zhang, K. R. Atkinson, R. H. Baughman, *Science* **2004**, *306*, 1358 – 1361.
[31] Q. Li, Y. Li, X. Zhang, S. B. Chikkannanavar, Y. Zhao, A. M. Dangelewicz, L. Zheng, S. Doorn, Q. Jia, D. E. Peterson, *Adv. Mater.* **2007**, *19*, 3358 – 3363.
[32] K. Koziol, J. Vilatela, A. Moisala, M. Motta, P. Cunniff, M. Sennett, A. Windle, *Science* **2007**, *318*, 1892 – 1895.
[33] A. B. Dalton, S. Collins, E. Munoz, J. M. Razal, V. H. Ebron, J. P. Ferraris, J. N. Coleman, B. G. Kim, R. H. Baughman, *Nature* **2003**, *423*, 703 – 703.
[34] H. Peng, *J. Am. Chem. Soc.* **2008**, *130*, 42 – 43.
[35] M. Duarte, A. Pilla, J. Sieben, C. Mayer, *Electrochem. Commun.* **2006**, *8*, 159 – 164.
[36] B. Seger, P. V. Kamat, *J. Phys. Chem. C* **2009**, *113*, 7990 – 7995.
[37] F. Gong, H. Wang, X. Xu, G. Zhou, Z. S. Wang, *J. Am. Chem. Soc.* **2012**, *134*, 10953 – 10958.
[38] E. Ramasamy, W. J. Lee, D. Y. Lee, J. S. Song, *Electrochem. Commun.* **2008**, *10*, 1087 – 1089.
[39] Z. Yang, T. Chen, R. He, G. Guan, H. Li, L. Qiu, H. Peng, *Adv. Mater.* **2011**, *23*, 5436 – 5439.